Hindawi
Adsorption Science & Technology
Volume 2022, Article ID 9222441, 13 pages
https://doi.org/10.1155/2022/9222441

Research Article

Adsorption-Based Removal of Sb (III) from Wastewater by Graphene Oxide-Modified Zirconium-Based Metal-Organic Framework Composites

Yilu Deng, Qiming Mao, Shuang Luo, Xiande Xie, and Lin Luo

College of Resources and Environment, Hunan Agricultural University, Changsha 410128, China

Correspondence should be addressed to Shuang Luo; shuangluo@hunau.edu.cn and Lin Luo; luolin@hunau.edu.cn

Received 4 February 2022; Accepted 9 April 2022; Published 9 May 2022

Academic Editor: George Kyzas

The treatment of Sb (III) wastewater produced from mining activities is uniquely challenging and has therefore garnered increasing attention. Here, an amino-modified zirconium-based metal-organic framework material (UiO-66-NH_2) and its composites were loaded onto graphene oxide (GO@UiO-66-NH_2) via the hydrothermal method, after which these materials were used to adsorb Sb (III) in mine wastewater. The effects of adsorption time, pH, initial Sb (III) concentration, temperature, and adsorbent dosage on the removal performance of Sb (III) were then investigated. The adsorption processes of Sb (III) were examined via adsorption kinetic, isotherm, and thermodynamic analyses. XRD, SEM, and FTIR analyses demonstrated the presence of a porous structure and high levels of oxygen-containing functional groups on the UiO-66-NH_2 and GO@UiO-66-NH_2 surfaces. During the Sb (III) adsorption process, the adsorption rates of UiO-66-NH_2 and GO@UiO-66-NH_2 were very fast in the first 10 minutes, and the adsorption equilibrium was achieved in 12 h, with the adsorption efficiencies of 91.76% and 93.79%, respectively. At a pH of 7.0, 25°C, an initial Sb (III) concentration of 100 mg/L, and an adsorbent dosage of 0.04 g/L, the maximum Sb (III) adsorption capacities of UiO-66-NH_2 and GO@UiO-66-NH_2 reached 39.23 mg/g and 61.07 mg/g, respectively. The adsorption process was accurately described by the Langmuir model, meaning that the Sb (III) was adsorbed through single-layer uniform adsorption. Moreover, the adsorption process was highly consistent with the pseudo-second-order model, which was indicative of spontaneous and endothermic chemical adsorption. Additionally, the Sb (III) removal efficiency could be maintained approximately 70% after sorption-desorption recycling four times. Therefore, our study provides an economical and effective method for the removal of Sb (III) in wastewater treatment.

1. Introduction

Mineral resources play an important role in industrial production and energy utilisation [1, 2]. However, the water pollution caused by the exploitation and utilisation of mineral resources has recently attracted widespread attention [3]. According to comprehensive statistics from relevant industries, mine wastewater has a low pH and high sulphate concentrations and contains a variety of heavy metal ions such as Cu^{2+}, Pb^{2+}, Zn^{2+}, Cd^{2+}, As^{3+}, Sb^{3+}, and Ni^{2+} [3–6]. Among these, the physical acidity of antimony (Sb) directly oxidises and destroys various stable trace metal elements and sulphides in mine soil, which in turn facilitates the dissolution of various heavy metal elements (e.g., Fe, Zn, Cu, Cd, and Mg) into mine wastewater [7]. Although Sb is not considered a class I and its toxicity is lower than that of class I pollutants such as Cr^{6+} and N^{i2+} under the same conditions, previous studies have reported that the trivalent antimony [Sb (III)] is more toxic than pentavalent antimony [Sb (V)]. Additionally, this pollutant readily causes acid-base imbalances in aquatic environments and salinisation in terrestrial environments [8]. Inhalation of Sb (III) may also cause adverse health effects such as acute liver and kidney dysfunction, pneumonia, and mucosal oedema [9, 10]. Therefore, effective measures must be taken swiftly to solve Sb (III) pollution.

Currently, the main methods to remove heavy metal contaminants from aqueous solutions are adsorption,

coagulation precipitation, ion exchange, and membrane separation [11–16]. Among these methods, coagulation sedimentation produces large amounts of Sb-containing sludge, which can potentially result in serious secondary pollution [16]. Membrane separation is widely used due to its high treatment efficiency, but associated costs and membrane fouling limit the widespread adoption of this technology [13]. Ion exchange has a high removal efficiency and good selectivity, but its treatment performance can be easily affected by other coexisting ions [17]. In contrast, adsorption is a cost-efficient method that can be easily implemented and allows for the recycling of adsorbents [14, 15, 18]. Therefore, this strategy is still among the most widely used and effective methods to remove Sb from wastewater. Previous studies have demonstrated that montmorillonite can effectively adsorb antimony acetate with an equilibrium adsorption capacity of 0.0997 mg/g, under the conditions at 120°C, and reaching adsorption equilibrium at 2 h [19]. Xi et al. reported that the Sb (III) and Sb (V) adsorption capacities of bentonite at 5–50°C and a pH of 6 were 0.036 mg/g and 0.032 mg/g, respectively [20]. These findings indicated that the adsorption performance of adsorbents for Sb needs to be improved.

Metal-organic frameworks (MOFs) are a new type of organic-inorganic metal hybrid porous composites that are characterised by their high porosity, large specific surface area, and easily manipulated structure [21, 22]. These materials have been widely used in the field of water treatment to adsorb dyes and heavy metal ions, as well as for the photodegradation of organic pollutants. Wang et al. reported that a zirconium-based MOF (UiO-66) exhibited a very high As (V) removal performance, with adsorption capacity reaching 303.4 mg/g [23]. Shao et al. found that the introduction of $-NH_2$ into MOFs increased the adsorption capacity of the materials to up to 93.69 mg/g based on the adsorption of Hg^{2+} ions, which constituted a 500-fold improvement compared to the parent MOF material [24]. Additionally, UiO-66 and UiO-66-NH_2 have good stability under acidic conditions, as well as excellent Sb and As removal performance [25]. These findings demonstrate that UiO-66 and UiO-66-NH_2 are good candidates for the removal of Sb from acid mine wastewater. However, the UiO-66 and UiO-66-NH_2 cannot be easily recovered from aqueous solutions due to their powder form. To address this limitation, these zirconium-based MOFs could be fixed on a simple and cost-effective carrier.

Graphene oxide (GO) is a porous nanomaterial that is characterised by its low price, large specific surface area, good dispersion properties, and abundance of oxygen-containing functional groups [26, 27]. GO has proven to be a good carrier because the properties of its surface can be modified through chemical functionalisation, in addition to being cost-efficient and highly stable [28]. For example, GO-iminodiacetic acid and GO-glycine were successfully synthesised and used as a carrier for novel drugs by Violetta et al. [28]. Furthermore, Wu et al. prepared a composite by loading cetylpyridinium bromide onto a GO carrier and reported that the composite had good antibacterial activity and reduced the cytotoxicity of cetylpyridinium bromide [29]. Additionally, the adsorbent could efficiently remove a variety of water pollutants such as herbicides, pesticides, phenols, dyes, heavy metals, and sulphonamides [30–33]. Therefore, Sb could be efficiently and cost-effectively removed from acid mine wastewater using a novel composite adsorbent material synthesised through the modification of GO and zirconium-based MOFs. GO and MOFs are considered promising heavy metal adsorbents due to their excellent physical and chemical properties [21]. However, the removal performances and mechanisms of GO and MOF composites for Sb adsorption need to be further explored.

Therefore, this study prepared two novel adsorption materials, namely, an amino-modified zirconium-based metal-organic framework material (UiO-66-NH_2) and its composites loaded with graphene oxide (GO@UiO-66-NH_2), after which their performance for the treatment of simulated Sb-containing wastewater was evaluated. The Sb (III) adsorption properties and mechanisms of the prepared materials were comprehensively explored through material characterisation analysis and adsorption equilibrium isotherm fitting, as well as thermodynamic and kinetic analyses. The outcomes of this study could thus provide an economical and effective method for the treatment of Sb-containing mine wastewater.

2. Materials and Methods

2.1. Chemicals. Analytical grade graphite powder and terephthalic acid (PTA) were purchased from McLean. Analytical grade zirconium chloride ($ZrCl_4$), 2-aminoterephthalic acid (2-HN_2-HBDC), and N,N-dimethylformamide (DMF) were procured from Aladdin, and analytical grade sulfuric acid (H_2SO_4), hydrochloric acid (HCl), sodium hydroxide (NaOH), potassium permanganate ($KMnO_4$), antimony potassium tartrate ($C_8H_4K_2O_{12}Sb_2$), hydrogen peroxide (H_2O_2), and methanol were purchased from Sinopharm Chemical Reagent Co., Ltd. (Shanghai, China). All experiments were conducted using ultrapure water.

2.2. Synthesis of the Adsorbents

2.2.1. Preparation of GO. In an ice bath at 20°C, 500 mg of graphite powder was added to a flask, followed by 65 mL of H_2SO_4. Next, 3 g $KMnO_4$ was weighed and ground in a mortar, after which it was gradually and slowly added to the above-described solution. The preparation was continuously stirred for three days with a magnetic stirrer until complete graphite oxidation [34]. Ultrasonic treatment was conducted when the colour of the solution changed from dark purple to green and finally black-brown. Afterwards, an appropriate amount of H_2O_2 solution (30%) was added drop by drop until the solution turned bright yellow, indicating that the graphene was sufficiently oxidised. Next, the product was centrifuged and washed with 1 mol/L HCl and abundant deionised water until the pH of the obtained product was 4–5. The product was then redispersed in deionised water for 2 h, after which a GO gel was obtained. The gel was dialysed for one week, then freeze-dried to obtain GO.

2.2.2. Synthesis of UiO-66 and UiO-66-HN_2. 0.2332 g of $ZrCl_4$ and 0.1664 g of PTA were added into a 100 mL conical flask and evenly dissolved in 50 mL of DMF solution. Ultrasonic treatment was then performed until the solution was completely dispersed, at which point it was transferred to an autoclave and allowed to react at 120°C for 48 h. Once the autoclave was naturally cooled to room temperature, the obtained product was washed with DMF solution and methanol, centrifuged for five times, and vacuum dried at 90°C for 12 h to obtain UiO-66 [35]. UiO-66-NH_2 was prepared in the same way as UiO-66, except that PTA (0.1664 g) was replaced with 2-NH_2-HBDC (0.1802 g).

2.2.3. Preparation of GO@UiO-66-NH_2 Composites. 10 mg of GO and 50 mL of DMF solution were added into a 100 mL conical flask, and ultrasonic dispersion treatment was conducted for 1 h. Next, 0.2332 g $ZrCl_4$ and 0.1802 g NH_2-HBDC were added when the solution was completely transparent, followed by ultrasonic treatment for 10 min when the solution had completely dissolved. The mixed solution was then transferred to an autoclave and allowed to react at 120°C for 48 h. Once the autoclave cooled to room temperature, the product was washed with DMF and methanol and centrifuged five times, sealed and soaked in a methanol solution at room temperature for 3 days, and dried in a vacuum chamber at 90°C for 12 h, after which the GO@UiO-66-NH_2 composites were obtained [21].

2.3. Adsorption Experiments

2.3.1. Single-Factor Experiment. Batch experiments were conducted with simulated Sb-containing wastewater. A 1 g/L Sb (III) stock solution was prepared using $C_8H_4K_2O_{12}Sb_2$, after which this solution was diluted to the desired concentrations according to the experimental requirements. The effects of single factors such as adsorption time, temperature, adsorbent dosage, initial Sb (III) concentration, and the pH value of the solution on the adsorption properties of the materials were then investigated. The adsorption reaction system consisted of 100 mL of Sb (III) solution. The pH value was adjusted using 1.0 mol/L HCl and 1.0 mol/L NaOH. A certain amount of adsorbent was accurately weighed and added to the solution, after which the adsorption experiment was conducted in a constant temperature oscillator at a certain temperature. A small number of water samples were regularly extracted and filtered using a 0.22 μm microporous filter, and the supernatant was used to determine the concentration of Sb (III). Batch experiments were conducted at various initial concentrations of Sb (5–100 mg/L), adsorbent dosages (0.01–0.08 g/L), adsorption times (10–1440 min), initial pH values (2.5–9.5), and temperatures (15–35°C). Three parallel experiments were conducted for each group. The adsorption performance of the prepared adsorbents was evaluated in terms of their Sb (III) removal efficiency [Equation (1)] and adsorption capacity [Equation (2)] [36]:

$$\eta = \frac{C_0 - C_t}{C_0} \times 100\%, \tag{1}$$

$$q_t = \frac{(C_0 - C_t)V}{m}, \tag{2}$$

where η (%) is the removal efficiency, C_0 (mg/L) is the initial concentration of Sb (III), C_t (mg/L) is the concentration of Sb (III) after adsorption for t min, q_t (mg/g) is the adsorption capacity after adsorption for t min, V (L) is the volume of the reaction solution, and m (g) is the dosage of the adsorbents.

2.3.2. Adsorption Kinetics, Thermodynamics, and Adsorption Equilibrium Isotherms. Adsorption kinetic analyses were performed to better understand the Sb (III) adsorption processes and mechanisms of the prepared materials. The obtained data were fitted and analysed using the pseudo-first-order model [Equation (3)], pseudo-second-order model [Equation (4)], W-M internal diffusion model [Equation (5)], and Elovich kinetic model [Equation (6)] [23]:

$$\ln (q_e - q_t) = \ln q_e - k_1 t, \tag{3}$$

$$\frac{t}{q_t} = \frac{1}{k_2 {q_e}^2} + \frac{t}{q_e}, \tag{4}$$

$$q_t = k_p t^{1/2} + c, \tag{5}$$

$$q_t = a + b \ln t, \tag{6}$$

where q_e (mg/g) is the equilibrium sorption amount of Sb (III) on the sorbents; t (min) is the adsorption time; K_1 (min^{-1}), K_2 ($g{\cdot}mg^{-1}{\cdot}min^{-1}$), and K_P are the rate constants of the adsorption reaction in the pseudo-first-order, pseudo-second-order, and W-M internal diffusion models, respectively; and a, b, and c are constants.

To obtain the maximum saturated adsorption capacity of the adsorbents, the adsorption equilibrium experiments were conducted and the experimental results were fitted and analysed using the Freundlich adsorption isotherm [Equation (7)], Langmuir adsorption isotherm [Equation (8)], Temkin adsorption isotherm [Equation (9)], and Dubinin-Radushkevich adsorption isotherm models [Equation (10)] [20].

$$\ln q = \ln K + \frac{1}{n} \ln C_t \tag{7}$$

$$\frac{1}{q} = \frac{1}{q_e} + \frac{1}{b q_e c_t} \tag{8}$$

$$q = B_1 \ln K_t + B_1 \ln C_t \tag{9}$$

$$\ln q = \ln q_e - B\varepsilon^2, \tag{10}$$

where q (mg/g) is the adsorption amount of Sb (III) on the adsorbents, C_t (mg/L) is the concentration of Sb (III) in the solution at adsorption equilibrium, and K, $1/n$, and B are adsorption constants.

To better clarify the Sb (III) adsorption and removal process of the adsorbent, thermodynamic analyses were conducted when studying the effect of temperature on Sb (III) removal. The coefficient K_d related to temperature and

adsorption thermodynamic parameters (ΔG_0, ΔS_0, ΔH_0) was calculated through the following equations [19, 20].

$$K_d = \frac{q}{C_t},$$
$$\ln K_d = \frac{\Delta S_0}{R} - \frac{\Delta H_0}{RT}, \quad (11)$$
$$\Delta G_0 = \Delta H_0 - T\Delta S_0,$$

where R [8.314 J/(mol·K)] is the gas constant and T (K) is the absolute temperature of the solution.

2.3.3. Influence of Coexisting Ions. Although relatively friendly to the environment, the large number of anions in acid mine wastewater may compete with Sb (III) for specific adsorption sites on the adsorption materials [36]. The most common impurity ions in acid mine wastewater include SO_4^{2-}, Cl^-, NO_3^-, HPO_4^{2-}, and $H_2PO_4^-$. Therefore, our study sought to characterise the effects of these ions on Sb (III) adsorption. Based on the results of our single factor experiments, the interaction and influence of coexisting ions on Sb (III) were studied under optimal conditions when the concentrations of SO_4^{2-}, Cl^-, NO_3^-, HPO_4^{2-}, and $H_2PO_4^-$ were 0.1 mol/L.

2.3.4. Recycling Experiment. Regeneration and reusability are critical parameters to determine the industrial application of adsorbents, and therefore, these parameters were investigated in this study. 100 mL NaOH solution with a concentration of 1.0 mol/L was used to desorb the saturated adsorbents, after which the adsorbents were washed with ultrapure water until neutral. The adsorbents were then dried and reused for Sb (III) adsorption to evaluate their potential practical application.

2.4. Analytical Methods and Characterisation. The concentration of Sb (III) was determined using an atomic absorption spectrophotometer (AA6000, Shimadzu Corporation). The structures of UiO-66, UiO-66-NH_2, and GO@UiO-66-NH_2 were characterised by X-ray diffraction (XRD-6100, Shimadzu Corporation) at a scanning rate of 4°/min and a scanning range of 5–80° [37]. The FTIR spectra of the prepared adsorbents were obtained with a Fourier-transform infrared spectrometer (ALPHA, Bruker, Germany) using the KBr pellet method. Additionally, the morphology of the prepared adsorbents was determined by scanning electron microscopy (SEM) (FESEM, Hitachi SU8220, Japan) [38].

3. Results and Discussion

3.1. Characterisation Analysis of the Prepared Adsorbents. XRD characterisation of UiO-66, UiO-66-NH_2, and GO@UiO-66-NH_2 was conducted to understand the crystal structure of zirconium-based MOF materials and their modified composites. As shown in Figure 1(a), a characteristic linear diffraction peak of UiO-66-NH_2 was observed at a 5–10° range and the XRD pattern was very similar to that of UiO-66, indicating that the structure of UiO-66 was not affected by the modification of coordination crystals with the introduction of an amino acid [39]. A typical linear diffraction peak of GO was observed at the diffraction position of 5–10° at 2θ. GO@UiO-66-NH_2 exhibited a clearly similar XRD pattern with UiO-66 and UiO-66-NH_2, and a higher diffraction intensity at the 5–10° position [35]. These findings suggested that the structure of UiO-66-NH_2 in GO@UiO-66-NH_2 was also not damaged or altered, which was consistent with previous studies.

Moreover, SEM analysis was performed on UiO-66, UiO-66-NH_2, GO, and GO@UiO-66-NH_2 to characterise the microstructure of the prepared materials before and after modification and the generation of composites (Figure S1). The UiO-66 crystals were randomly aggregated and had an octahedral nanostructure (Figure S1a), which was in good agreement with the findings of Lu et al. [40]. Moreover, UiO-66 also exhibited a porous structure. UiO-66-NH_2 was prepared after the ligand was replaced by the amino group. It still had the same structure as UiO-66, but the crystal arrangement was closer, and the surface was coarser than that of UiO-66 (Figure S1b). This might be because the amino group on the ligand did not coordinate with the metal ion cluster in the MOF structures [41]. The SEM image of GO showed that GO had an interconnected porous network structure (Figure S1c). As the main basal chain of the composite, the porous network structure of GO can provide a larger specific surface area, abundant open active sites, and good ductility, all of which can facilitate the binding of functional materials such as UiO-66-NH_2 crystal particles and compounds to form GO@UiO-66-NH_2 composite materials. A SEM image of GO@UiO-66-NH_2 is shown in Figure S1d. As observed in the image, the UiO-66-NH_2 crystals were randomly dispersed on the surface of GO and the porous network structure of GO could also be seen, indicating that UiO-66-NH_2 crystals successfully grew on GO [21], and the composite material (GO@UiO-66-NH_2) was successfully prepared.

Moreover, to further study the surface characteristics of the prepared adsorbents, UiO-66, UiO-66-NH_2, GO, and GO@UiO-66-NH_2 were analysed by FTIR (Figure 1(b)). The bending height stretching waveform vibration peaks of UiO-66 and UiO-66-NH_2 were similar. However, there was a C-N waveform stretching bending waveform vibration peak at 1256 cm^{-1} from the FTRIR curve of UiO-66-NH_2 [35]. Additionally, the bending vibration peaks located at 1577 cm^{-1} and 1401 cm^{-1} were the characteristic peaks of N-H [39, 42], whereas the stretching vibration peak at 3446 cm^{-1} was attributed to -NH_2. The appearance of these vibration peaks indicated the occurrence of -NH_2 in the structure of UiO-66-NH_2, and the introduced -NH_2 did not coordinate with metal ions but extended into the structural micropores. As for the FTIR spectrum of GO, the characteristic peak at 1097 cm^{-1} was ascribed to the stretching vibration peak of C-O, the characteristic peak at 1224 cm^{-1} was attributed to the epoxy absorption peak on the GO surface, the peaks at 1629 cm^{-1} and 1740 cm^{-1} represented the stretching vibration peaks of C=O, and the peak at 3419 cm^{-1} was ascribed to the stretching vibration peak of OH [21, 43]. Based on these peak patterns, we inferred that

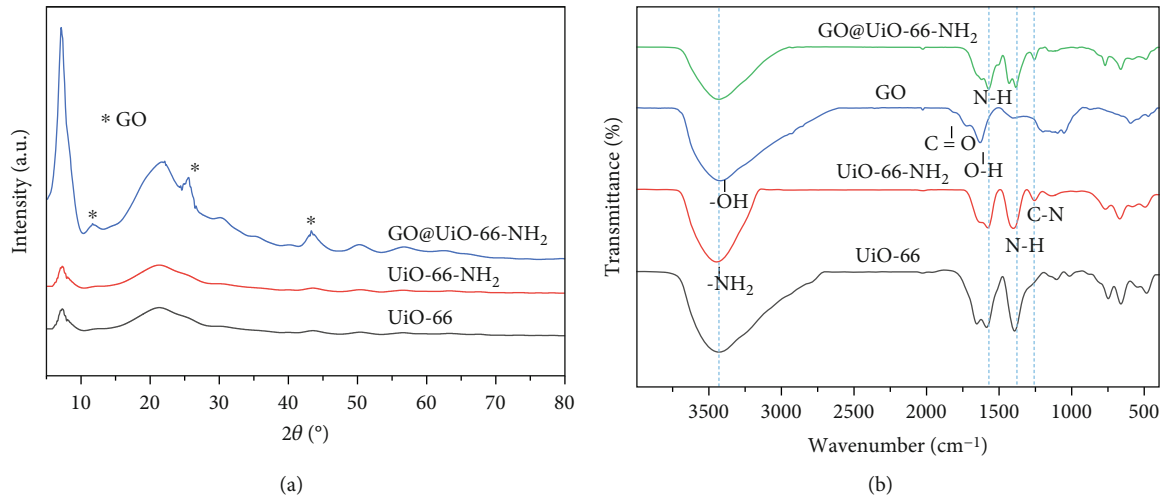

Figure 1: (a) XRD pattern of the prepared materials; (b) FTIR spectra of the prepared materials.

the newly introduced -NH_2 might form a hydrogen bond with -OH groups on the surface of GO. Additionally, it is worth noting that the FTIR spectrum of GO@UiO-66-NH_2 was similar to that of UiO-66-NH_2, suggesting that the composites of GO and UiO-66-NH_2 did not affect the structure and surface functional groups of UiO-66-NH_2. The variety of functional groups on the surface of the prepared composites could thus provide more active sites for pollutants [36].

3.2. Effect of Reaction Conditions on Sb (III) Adsorption

3.2.1. Determination of Adsorption Equilibrium Time. First, the effect of adsorption time on Sb (III) removal performance was investigated to determine the adsorption equilibrium time of UiO-66-NH_2 and GO@UiO-66-NH_2 composites for Sb (III). As illustrated in Figures 2(a) and 2(b), both UiO-66-NH_2 (a MOF-modified material) and GO@UiO-66-NH_2 (a MOF-composited material) had good adsorption capacity for Sb (III) and exhibited fast adsorption rates. When the initial concentration of Sb (III) was 10 mg/L, the removal efficiency of Sb (III) by UiO-66-NH_2 and GO@UiO-66-NH_2 reached 81.62% and 85.14% in 10 min, respectively. Afterwards, the adsorption removal efficiency and adsorption capacity increased gradually with adsorption time. Finally, the adsorption reactions of the two prepared materials reached equilibrium in 12 h. The removal efficiency and adsorption capacity of Sb (III) by UiO-66-NH_2 were 91.76% and 19.39 mg/g, respectively, whereas the removal efficiency and adsorption capacity of Sb (III) by GO@UiO-66-NH_2 were 93.79% and 19.82 mg/g, respectively. These values were orders of magnitude higher than those achieved by montmorillonite (0.0997 mg/g) and bentonite (0.036 mg/g), as reported by Zhao et al. and Xi et al., respectively (Table S1).

As indicated by our experimental results, GO@UiO-66-NH_2 had better adsorption capacity than UiO-66-NH_2, which was attributed to the large amounts of functional groups on the surface of GO, as well as its porous structure with a large specific surface area. Therefore, GO improved the Sb (III) adsorption performance of the adsorbent. Moreover, in the initial adsorption stage, Sb (III) was quickly transferred from the liquid phase to the surface of the adsorption material. This was because the Zr-O bond in UiO-66-NH_2 has a certain specificity for the adsorption of Sb (III) [23, 44]. Afterwards, the adsorption rate of Sb (III) slowed down after 2 h of adsorption. In this stage, the functional groups on the surface of GO and its rich layered structure reacted with Sb (III) [45], and Sb (III) also slowly diffused to the internal pores of GO@UiO-66-NH_2. Finally, the adsorption reached equilibrium at 12 h.

3.2.2. Effect of Adsorbent Dosage on Sb (III) Adsorption. Generally, a higher adsorbent dosage translates to more adsorption active sites for pollutants to bind [46]. However, excessive adsorbent input can not only increase treatment costs but also make the retrieval of the adsorbents more challenging and even lead to secondary pollution. In contrast, if the adsorbent dosage is too low, the pollutants in the wastewater cannot be efficiently removed. Therefore, it is very important to select an optimal dosage of adsorbents in practical application to minimise costs while maximising effectiveness. This study thus explored the effect of the dosages of adsorption materials on their adsorption performance, and the results are shown in Figures 2(c) and 2(d).

As shown in Figures 2(c) and 2(d), the adsorption capacity of Sb (III) decreased gradually with increasing adsorbent dosage, with the Sb (III) adsorption capacity of UiO-66-NH_2 and GO@UiO-66-NH_2 decreasing from 49.59 to 9.59 mg/g and from 60.27 to 10.48 mg/g, respectively. This may result from the overlapping or aggregation of adsorption sites, which resulted in a decrease in the total adsorbent surface area available to metal ions and an increase in the diffusion path length [46]. However, the removal efficiency of Sb (III) increased at higher adsorbent dosages. For the adsorption of Sb (III) by UiO-66-NH_2, the removal efficiency was stable when the dosage was 0.08 g/L and the removal efficiency was 89.26%. For GO@UiO-66-NH_2, the removal efficiency was stable when the dosage was 0.04 g/L and the removal efficiency reached 93.47%. This was because the prepared materials had octahedral cubic structures

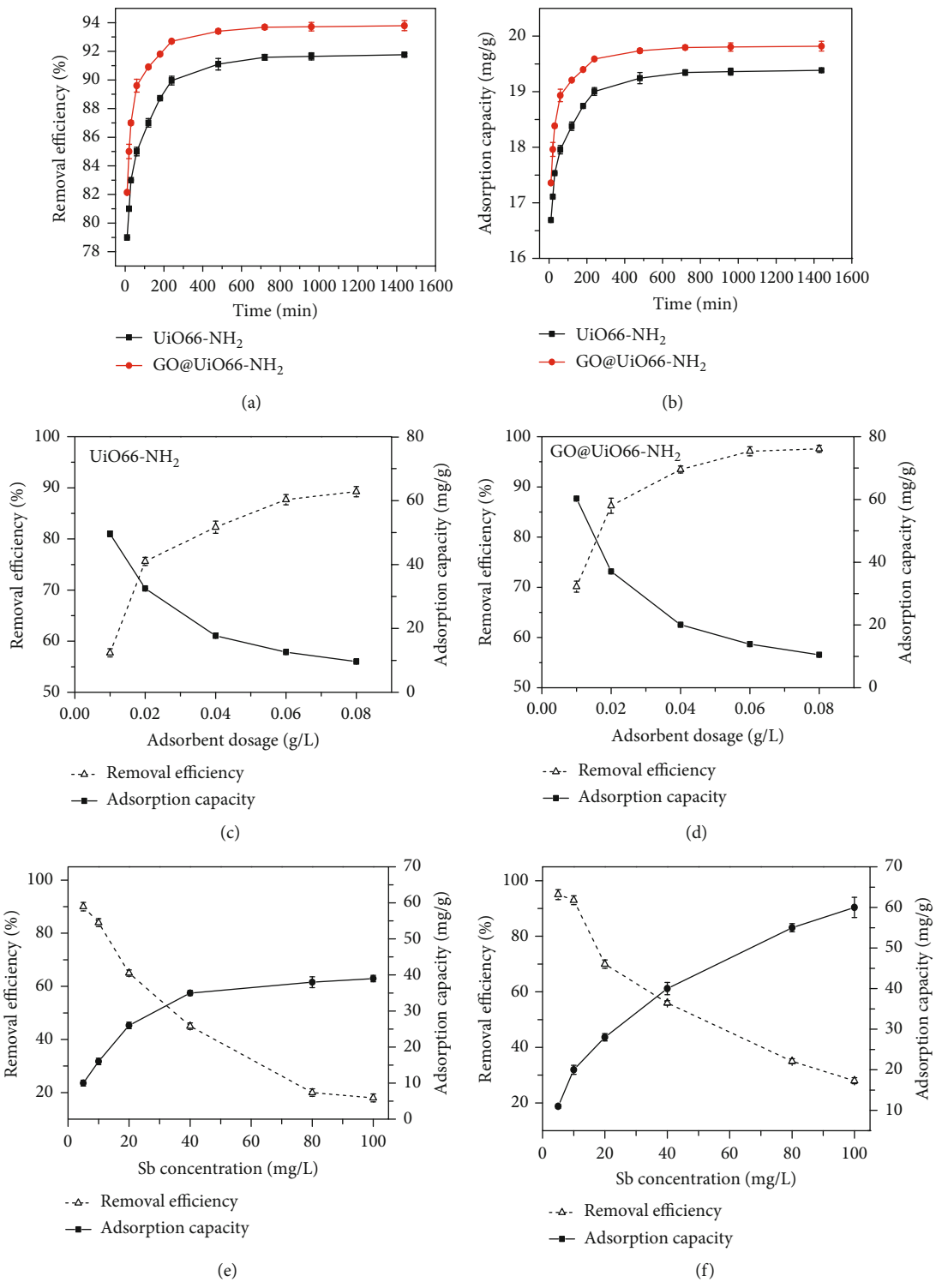

Figure 2: The effect of contact time on the adsorption removal efficiency (a) and adsorption capacity (b); the effect of adsorbent dosage on the adsorption of Sb (III) by UiO-66-NH_2 (c) and GO@UiO-66-NH_2 (d); the effect of initial Sb (III) concentration on the adsorption of Sb (III) by UiO-66-NH_2 (e) and GO@UiO-66-NH_2 (f).

composed of Zr-O bonds. When the concentration of Sb (III) was constant, increasing the input of adsorbents could increase the number of unsaturated adsorption sites on the surface of the adsorbents, and more Zr-O bonds could combine with Sb (III) to improve the removal efficiency of Sb (III). Additionally, for the GO@UiO-66-NH_2 composites, due to the uniform growth of UiO-66-NH_2 on GO, GO@UiO-66-NH_2 had a higher specific surface area and porous structure, which provided more active sites and mass transfer. Therefore, the removal efficiency of Sb (III) by

GO@UiO-66-NH_2 was higher than that of UiO-66-NH_2. When the dosage of adsorption materials continued to increase, the Sb (III) in the solution decreased gradually and the removal rate increased slowly until stable.

3.2.3. Effect of Initial Concentration on Sb (III) Adsorption. In practice, due to the leaching of rainwater and the large variations in Sb content in different mines, the effect of the initial concentration of Sb (III) at 5–100 mg/L on the adsorption performance of the adsorbents was investigated in this study. The experimental results are shown in Figures 2(e) and 2(f).

As illustrated in Figures 2(e) and 2(f), as the initial Sb (III) concentration increased, the removal efficiency of Sb (III) by UiO-66-NH_2 decreased from 89.93% to 18.58%, whereas the adsorption capacity increased from 9.79 to 39.23 mg/g. For GO@UiO-66-NH_2, the removal efficiency decreased from 96.23% to 28.30% under the same conditions, whereas the adsorption capacity increased from 9.79 to 61.07 mg/g. This was because the number of active sites on the material's surface was much higher than that on Sb (III) when the initial concentration of Sb (III) was low [47], which made the adsorbents reach a higher removal efficiency. With higher Sb (III) concentrations, the active sites (Zr-O bond) on the material's surface were gradually occupied and combined with $H_2SbO_3^-$ to achieve adsorption equilibrium, and the adsorption capacity gradually increased to the corresponding equilibrium adsorption capacity [35].

We thus concluded that both UiO-66-NH_2 and GO@UiO-66-NH_2 had good Sb (III) adsorption performance and the Zr-O bond in the materials played a major role in the adsorption of Sb (III). The Sb (III) adsorption performance of GO@UiO-66-NH_2 was more stable than that of UiO-66-NH_2, and the adsorption effect of GO@UiO-66-NH_2 on Sb (III) exceeded 93.79% at low concentrations (5 mg/L, 10 mg/L). Therefore, we concluded that the optimal initial concentration of Sb (III) was 5–10 mg/L.

3.2.4. Effect of pH on Sb (III) Adsorption. pH, a physical quality of water, has an important impact on the morphology of coexisting ions. H^+ or OH^- might occupy a certain adsorption site in the process of adsorption reaction. This changes the surface charge of adsorbents, which in turn affects their adsorption performance. Therefore, a pH range of 2.5–9.5 was selected to explore the effect of pH on UiO-66-NH_2 and GO@UiO-66-NH_2, and the results are shown in Figure 3(a).

As shown in Figure 3(a), both UiO-66-NH_2 and GO@UiO-66-NH_2 could effectively remove Sb (III) in a wide pH range. pH had little effect on the adsorption of Sb (III) in the selected pH range, and the two materials showed a good Sb (III) adsorption effect under acidic conditions. When the pH was 2.5–9.5, Sb (III) mainly existed in the form of $Sb(OH)_3$ and $Sb(OH)_4^-$ with very high solubility. Through electrostatic adsorption, the surfaces of UiO-66-NH_2 and GO@UiO-66-NH_2 were positively charged due to surface protonation and by combining with anions containing Sb (III) [45].The charge on the surface of the materials changed with the pH value in the solution, and the attraction to anions containing Sb (III) increased with the increase of positively charged sites. When the pH was higher than 7, hydroxide ions (OH^-) occupied some active sites of the adsorption materials. The negative charge on the surface of the adsorption materials increased and the electrostatic repulsion force with anions containing Sb (III) also increased, resulting in a gradual decrease in adsorption capacity. The maximum adsorption capacities of UiO-66-NH_2 and GO@UiO-66-NH_2 were 5.58 mg/g (at pH 6.5) and 6.07 mg/g (at pH 4.5), respectively. When the pH value was 8.5 or 9.5, the Sb (III) adsorption capacity of UiO-66-NH_2 was 5.05 mg/g and 5.07 mg/g, respectively. Similarly, the Sb (III) adsorption capacity of GO@UiO-66-NH_2 was 5.58 mg/g and 5.60 mg/g, respectively. This was because the Zr-O bond in the two prepared materials was stable in both acidic and alkaline environments, and therefore, increasing the pH value had little effect on adsorption [44]. This result was also consistent with the findings of Qi et al. [39].

Additionally, the zero-charge value pH_{pzc} of UiO-66-NH_2 was 8.5. When $pH < pH_{pzc}$, the surface of UiO-66-NH_2 was positively charged due to the protonation reaction. In contrast, OH^- would be adsorbed through hydrogen bonding at high pH conditions, and the surface charge would become negative. Due to the electrostatic repulsion under strong alkalinity, the adsorption capacity of the materials for Sb (III) was relatively low. Therefore, the prepared materials adsorbed Sb (III) more effectively under acidic conditions.

Compared with the adsorption of Sb (III) by Fe_3O_4@TA@UiO-66 studied by Qi et al. [39], the removal efficiency of Sb (III) in acidic and neutral solutions was approximately 80% at an absorbent dosage of 0.2 g/L and initial concentration of 10 mg/L. In this experiment, the maximum removal efficiency of Sb (III) by the prepared materials reached 99.10% at an absorbent dosage of 0.04 g/L and an initial concentration of 10 mg/L. As summarised in Table S2, our analyses of the adsorption capacity of Sb (III) by the prepared materials at different pH values indicated that there was no significant difference between the experimental conditions ($P > 0.05$), meaning that the adsorption materials developed in this study could effectively remove Sb (III) in acid mine wastewater.

3.2.5. Effect of Temperature on Sb (III) Adsorption. Temperature is not only an important parameter affecting the Brownian motion of pollutant molecules but also an important physical parameter that affects the adsorption and desorption of pollutant molecules on the adsorbent surface [43, 48]. Therefore, this study explored the effects of different temperatures on the adsorption performance of the adsorbents for Sb (III), and the results are shown in Figure 3(b).

At higher adsorption temperatures, the removal efficiency of Sb (III) by UiO-66-NH_2 and GO@UiO-66-NH_2 increased gradually. When the temperature was 15–30°C, the removal efficiency of Sb (III) by UiO-66-NH_2 and GO@UiO-66-NH_2 gradually increased from 91.6% to 98.3% and from 97.5% to 99.5%, respectively, indicating that this temperature range favoured the adsorption reaction, and the adsorption reaction was endothermic.

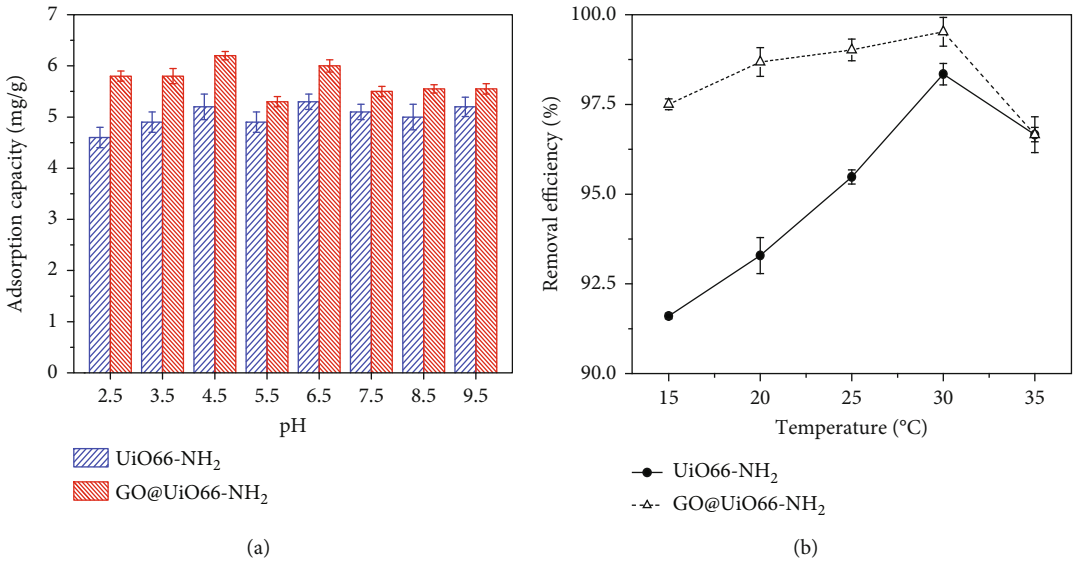

Figure 3: The effect of pH (a) and temperature (b) on the adsorption of Sb (III) by UiO-66-NH_2 and GO@UiO-66-NH_2.

When the temperature increased to 35°C, the adsorption removal efficiency of the two materials decreased to 96.6%. The removal efficiency of GO@UiO-66-NH_2 was reduced by approximately 2.9% compared with that at 25°C. Based on these results, we inferred that the oxygen-containing functional groups on the GO surface and the Zr-O bond on MOFs were more likely to combine with $H_2SbO_3^-$ when the temperature increased due to the endothermic nature of the reaction. Moreover, the increase in temperature can improve the solubility of metals [36, 48], reduce the adsorption sites on the adsorption materials, and degrade the original structure of the materials [49], thus affecting the adsorption of Sb (III) by GO@UiO-66-NH_2. Overall, temperature changes had little effect on the removal of Sb (III) by UiO-66-NH_2 and GO@UiO-66-NH_2. Therefore, the two adsorbents prepared in this study have good application prospects because they can maintain good adsorption performance even at low temperatures (15–25°C), especially GO@UiO-66-NH_2, which has an Sb (III) removal efficiency of 97.5% at 15°C. Given that temperature did not affect sorption, all subsequent experiments were conducted at room temperature (25°C).

Based on our findings, the optimal operating parameters for the adsorption and removal of Sb (III) from acid mine wastewater were as follows: Sb (III) initial concentration of 5–10 mg/L, adsorbent dosage of 0.04 g/L, 25°C temperature, natural pH, and the adsorption equilibrium time was 12 h.

3.3. Influence of Coexisting Ions and Adsorption Regeneration Experiment

3.3.1. Influence of Coexisting Ions on Sb (III) Adsorption. Under the optimum operating conditions, this study explored the effects of five anions (SO_4^{2-}, Cl^-, NO_3^-, HPO_4^{2-}, and $H_2PO_4^-$) that commonly occur in acid mine wastewater on the adsorption performance of the adsorbents (Figure 4). Our findings indicated that the occurrence of coexisting anions had no significant effect on the removal of Sb (III) by the materials. When there were no coexisting anions, the maximum adsorption capacities of UiO-66-NH_2 and GO@UiO-66-NH_2 were 14.93 and 17.87 mg/g, respectively. In the presence of NO_3^-, the Sb (III) adsorption capacity of UiO-66-NH_2 and GO@UiO-66-NH_2 decreased by 19.59% and 14.39%, respectively. However, in the presence of the other four anions, Sb (III) removal performance remained largely unaffected because these anions had no significant competition with Sb (III) on the surface adsorption sites of UiO-66-NH_2 and GO@UiO-66-NH_2 [39], and the adsorption of Sb (III) by UiO-66-NH_2 and GO@UiO-66-NH_2 was highly specific. UiO-66-NH_2 can effectively remove Sb (III) by relying on the action of the Zr-O bond, and the adsorption performance of Sb (III) was significantly enhanced after the combination of UiO-66-NH_2 and GO [21, 44].

3.3.2. Adsorption Regeneration Experiment. Adsorption regeneration experiments were conducted to study the regeneration stability and reusability of the prepared materials, which would provide insights into their potential practical applications. The results are shown in Figures 5(a) and 5(b).

After four adsorption-desorption cycles, the adsorption removal efficiency of UiO-66-NH_2 was 67.16%, which constituted 70.34% of its initial removal efficiency. Similarly, the removal efficiency of GO@UiO-66-NH_2 was 70.38%, representing 71.08% of the initial removal efficiency. These findings were consistent with those of He et al., who explored the As adsorption performance of UiO-66-NH_2 [50]. Moreover, our findings also indicated that graphene materials and zirconium-based MOFs possess good regeneration ability.

3.4. Adsorption Kinetics, Isotherm, and Thermodynamic Analyses

3.4.1. Analysis of Adsorption Kinetics. To gain further insights into the Sb (III) adsorption performance and

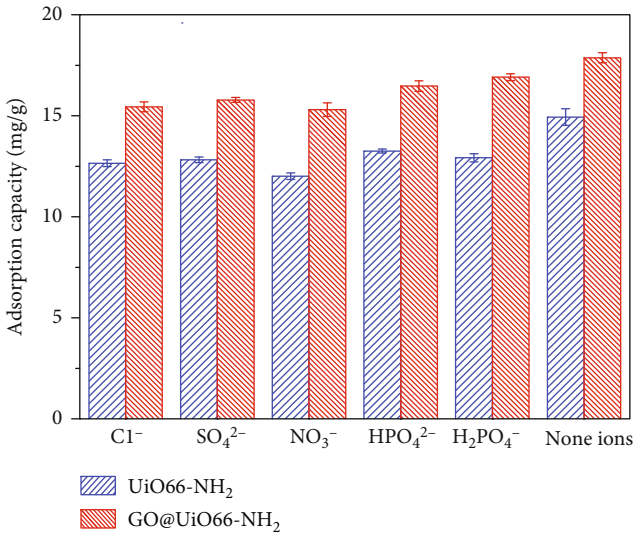

Figure 4: The effect of competing anions on the adsorption of Sb (III) on the prepared materials.

mechanisms of UiO-66-NH_2 and GO@UiO-66-NH_2, the experimental data were fitted and analysed using the pseudo-first-order, pseudo-second-order, W-M internal diffusion, and Elovich kinetic models. The fitting results of Sb (III) adsorbed by UiO-66-NH_2 and GO@UiO-66-NH_2 are shown in Figure S2, and the relevant adsorption kinetic parameters are summarised in Table S3.

The adsorption of Sb (III) by UiO-66-NH_2 and GO@UiO-66-NH_2 was more accurately described by the pseudo-second-order model equation [39], and the correlation coefficients reached 0.9999. In the pseudo-second-order kinetics, the theoretical equilibrium adsorption capacities of the two materials were 19.43 and 19.85 mg/g, respectively, whereas the equilibrium adsorption capacities obtained in experiment 3.2.1 were 19.39 and 19.82 mg/g, respectively, indicating that the theoretical equilibrium adsorption capacity of Sb (III) by UiO-66-NH_2 and GO@UiO-66-NH_2 was highly consistent with the actual experimental results.

Moreover, the R^2 values of the Elovich kinetic model fitted for UiO-66-NH_2 and GO@UiO-66-NH_2 were 0.9786 and 0.9718, respectively. Although the Elovich kinetic model did not make clear mechanism assumptions, it can be used to demonstrate that the surface adsorption of heterogeneous solids occurred mainly through chemical adsorption [36]. In turn, these results provided insights into the involvement of the surface structure of GO and UiO-66-NH_2 in the sorption process. When a large number of adsorption binding sites reacted with Sb (III), the activation energy changed greatly. Additionally, the R^2 values of the W-M internal diffusion model fitted for UiO-66-NH_2 and GO@UiO-66-NH_2 were 0.7549 and 0.7111, respectively (Figure S2, Table S3). This suggested that the relationship between q_t and t during the adsorption process was not linear, indicating that the adsorption process was not controlled by internal diffusion only (Moghimi et., [51]). Therefore, Sb (III) was removed from the aqueous solution through a chemical adsorption mechanism, as indicated by the pseudo-second-order models [36].

3.4.2. Adsorption Isotherms of Sb (III) by the Prepared Materials. Adsorption equilibrium experiments were conducted to obtain the removal efficiency and maximum saturated adsorption capacity of the adsorption materials. The experimental results were fitted and analysed via the Freundlich, Langmuir, Temkin, and Dubinin-Radushkevich adsorption isotherm models. The results and corresponding fitting parameters are shown in Figure 3, Figure 6, and Table S4, respectively.

The R^2 coefficients of UiO-66-NH_2 and GO@UiO-66-NH_2 based on the Freundlich isothermal equation were 0.87624 and 0.8342, respectively (Figure S3). In contrast, the R^2 fitting coefficients of UiO-66-NH_2 and GO@UiO-66-NH_2 according to the Langmuir isothermal equation were 0.9808 and 0.9270, respectively (Figure 6). Therefore, the adsorption of Sb (III) by UiO-66-NH_2 and GO@UiO-66-NH_2 was more consistent with the Langmuir adsorption isotherm, suggesting that the adsorption of Sb (III) in this study occurred mainly through monolayer adsorption [19].

The theoretical equilibrium adsorption capacities of the two materials calculated from the Langmuir isothermal equation were 16.32 and 19.19 mg/g, respectively, which were also close to the equilibrium adsorption capacities obtained in the experiment. Additionally, the value of b could be used to judge the stability of the binding between the adsorbents and Sb (III). The larger the value of b, the more stable the binding between them [52]. Furthermore, both UiO-66-NH_2 and GO@UiO-66-NH_2 had good adsorption performance for Sb (III). However, the adsorption of Sb (III) by GO@UiO-66-NH_2 was more stable during the adsorption process.

3.4.3. Adsorption Thermodynamics of Sb (III) by the Prepared Materials. To better clarify the adsorption process of the adsorbents on Sb (III), the adsorption thermodynamics were analysed when studying the effect of temperature on the adsorption performance of the adsorbents, and the results are shown in Figure S4 and Table S5.

According to the results in Figure S4 and the thermodynamic parameters in Table S5, the calculated values of ΔH_0 on UiO-66-NH_2 and GO@UiO-66-NH_2 for Sb (III) were 81.82 and 79.47 kJ/mol, respectively, indicating that the adsorption process between 15 and 30°C was an endothermic reaction. The calculated values of ΔS_0 were 304.08 and 308.16 J/(mol·K), respectively, suggesting that the degree of freedom of Sb (III) adsorption decreased. The calculated values of ΔG_0 were negative between 15 and 30°C, and ΔG_0 decreased with increasing adsorption temperature, indicating that the two materials spontaneously carried out adsorption reactions in the process of Sb (III) adsorption [20]. Within the studied temperature range (15–30°C), the reaction was more likely to proceed spontaneously at higher temperatures. Moreover, the adsorption process of UiO-66-NH_2 and

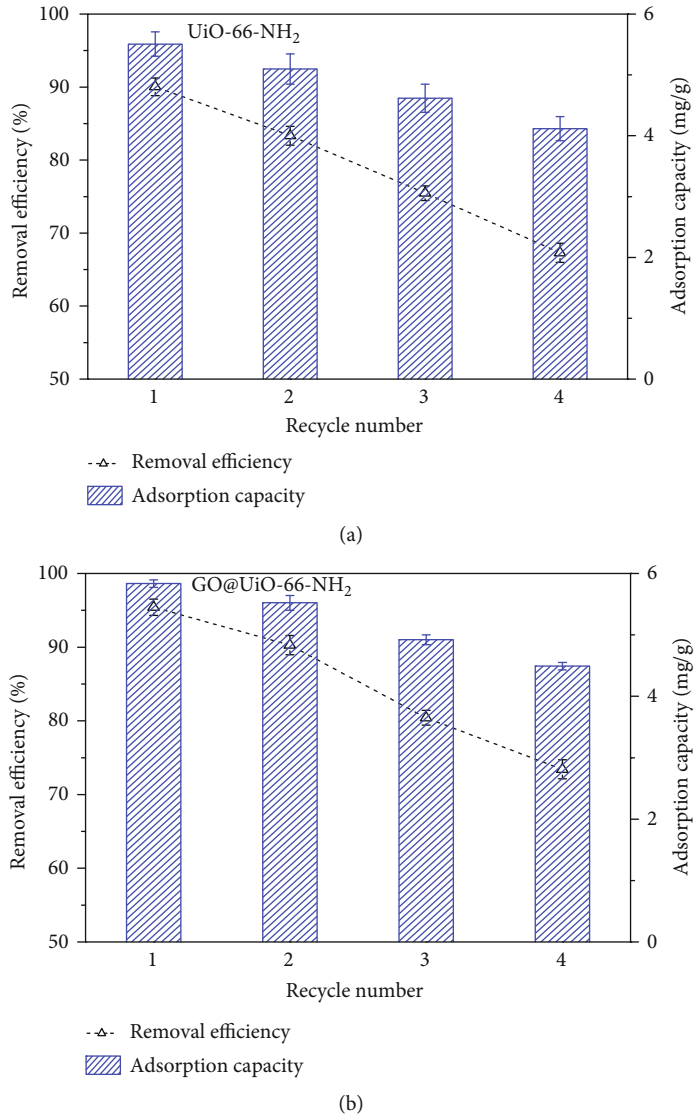

Figure 5: The desorption regeneration cycle effect diagram of UiO-66-NH_2 (a) and GO@UiO-66-NH_2 (b).

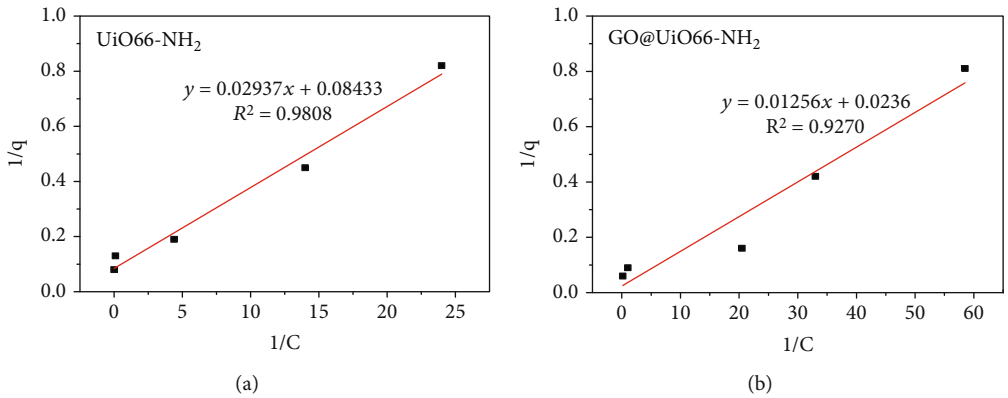

Figure 6: The Langmuir adsorption isotherms of (a) UiO-66-NH_2 and (b) GO@ UiO-66-NH_2 on Sb (III).

GO@UiO-66-NH_2 exhibited a similar trend, which was consistent with the conclusion obtained in the experiment described in Section 3.2.5. Therefore, our thermodynamic analyses suggested that the adsorption process of Sb (III) by the two materials was endothermic and spontaneous.

4. Conclusion

In this study, UiO-66-NH_2 and GO@UiO-66-NH_2 were successfully prepared and characterised. Next, we evaluated the capacity of the prepared materials to adsorb Sb (III), including their adsorption equilibrium isotherm, adsorption kinetics, and thermodynamics. The following are the main conclusions of this study:

(1) The introduction of -NH_2 did not change the basic structure and morphology of the zirconium-based MOF materials. Combining the materials with GO provided an abundance of functional groups and a porous structure with more active sites for the adsorption of Sb (III), thereby improving their Sb (III) adsorption performance

(2) The optimal operating parameters of the adsorbents prepared in this study for the removal of Sb (III) were as follows: initial Sb (III) concentration of 10 mg/L, natural pH, 25°C temperature, adsorption equilibrium time of 12 h, and adsorbent dosage of 0.04 g/L. The removal efficiencies of Sb (III) by UiO-66-NH_2 and GO@UiO-66-NH_2 were 91.93% and 94.13%, respectively, and the adsorption capacities reached 19.43 and 19.89 mg/g, respectively

(3) The adsorption mechanisms of Sb (III) by UiO-66-NH_2 and GO@UiO-66-NH_2 were more consistent with the Langmuir model, which was indicative of single-layer uniform adsorption. Both UiO-66-NH_2 and GO@UiO-66-NH_2 had good adsorption performance for Sb (III). However, GO@UiO-66-NH_2 exhibited higher stability and stronger adsorption properties

(4) The adsorption of the two materials for Sb (III) was in good agreement with the pseudo-second-order model, which aligned with a spontaneous and endothermic chemical adsorption mechanism. Additionally, the two adsorbent materials had good regeneration ability and reusability

The findings demonstrated that the materials prepared in this study are suitable for the treatment of Sb (III) from acid mine wastewater, thus providing an economical and effective method for the removal of Sb (III) from aquatic media.

Data Availability

All data generated or analysed during this study are included in this article.

Conflicts of Interest

The authors declare that they have no conflicts of interest.

Acknowledgments

Funding from the Hunan Provincial Key R&D (2018WK4007); National Natural Science Foundation of China (42077380); International Postdoctoral Exchange Fellowship Program 2021, China (PC2021020); and Science and Technology Innovation Program of Hunan Province, China (2020RC2053, 2021RC5006) is gratefully acknowledged.

Supplementary Materials

Supplementary data associated with this article can be found, in the online version. *(Supplementary Materials)*

References

[1] M. F. Cotrufo, M. G. Ranalli, M. L. Haddix, J. Six, and E. Lugato, "Soil carbon storage informed by particulate and mineral-associated organic matter," *Nature Geoscience*, vol. 12, no. 12, pp. 989–994, 2019.

[2] B. Q. Lin and R. Q. Zhu, "Energy efficiency of the mining sector in China, what are the main influence factors?," *Resources Conservation and Recycling*, vol. 167, no. 2, article 105321, 2021.

[3] L. Guo and T. J. Cutright, "Bioaccumulation of metals in reeds collected from an acid mine drainage contaminated site in winter and spring," *Environmental Technology*, vol. 37, no. 14, pp. 1821–1828, 2016.

[4] R. H. Li, L. Zhu, T. Tao, and B. Liu, "Phosphorus removal performance of acid mine drainage from wastewater," *Journal of Hazardous Materials*, vol. 190, no. 1-3, pp. 669–676, 2011.

[5] R. Xu, B. Q. Li, E. Z. Xiao et al., "Uncovering microbial responses to sharp geochemical gradients in a terrace contaminated by acid mine drainage," *Environmental Pollution*, vol. 261, article 114226, 2020.

[6] Y. J. Zhu, L. B. Zhou, Y. B. Zhu, and L. P. Ju, "Adsorption performance investigation of heavy metal copper in acid mine drainage by the Klebsiella oxytoca," *Legislation, Technology and Practice of Mine Land Reclamation*, vol. 1, no. 397, 2015.

[7] M. Jouini, C. M. Neculita, T. Genty, and M. Benzaazoua, "Environmental behavior of metal-rich residues from the passive treatment of acid mine drainage," *Science of the Total Environment*, vol. 712, article 136541, 2020.

[8] K. K. Kefeni and B. B. Mamba, "Evaluation of charcoal ash nanoparticles pollutant removal capacity from acid mine drainage rich in iron and sulfate," *Journal of Cleaner Production*, vol. 251, article 119720, 2020.

[9] V. Kumar, R. D. Parihar, A. Sharma et al., "Global evaluation of heavy metal content in surface water bodies: a meta-analysis using heavy metal pollution indices and multivariate statistical analyses," *Chemosphere*, vol. 236, article 124364, 2019.

[10] J. P. Vareda, A. J. M. Valente, and L. Duraes, "Assessment of heavy metal pollution from anthropogenic activities and remediation strategies: a review," *Journal of Hazardous Materials*, vol. 246, pp. 101–118, 2019.

[11] D. Balarak, A. Joghataei, H. Azarpira, and F. K. Mostafapour, "Isotherms and thermodynamics of CD (II) ion removal by adsorption onto Azolla Filiculoides International," *Journal of Pharmacy and Technology*, vol. 8, no. 3, pp. 15780–15788, 2016.

[12] E. Bazrafshan, M. Sobhanikia, F. K. Mostafapour, H. Kamani, and D. Balarak, "Chromium biosorption from aqueous environments by mucilaginous seeds of Cydonia oblonga: kinetic and thermodynamic studies," *Global NEST Journal*, vol. 19, no. 2, pp. 269–277, 2017.

[13] M. Kang, M. Kawasaki, S. Tamada, T. Kamei, and Y. Magara, "Effect of pH on the removal of arsenic and antimony using reverse osmosis membranes," *Desalination*, vol. 131, no. 1-3, pp. 293–298, 2000.

[14] A. H. Mahvi, D. Balarak, and E. Bazrafshan, "Remarkable reusability of magnetic Fe_3O_4-graphene oxide composite: a highly effective adsorbent for Cr (VI) ions," *International Journal of Environmental Analytical Chemistry*, pp. 1–21, 2021.

[15] T. A. Saleh, A. Sari, and M. Tuzen, "Effective adsorption of antimony(III) from aqueous solutions by polyamide-graphene composite as a novel adsorbent," *Chemical Engineering Journal*, vol. 307, pp. 230–238, 2017.

[16] Z. Wu, M. He, X. Guo, and R. Zhou, "Removal of antimony (III) and antimony (V) from drinking water by ferric chloride coagulation: competing ion effect and the mechanism analysis," *Separation and Purification Technology*, vol. 76, no. 2, pp. 184–190, 2010.

[17] S. H. Dong, C. X. Li, X. L. Ge, Z. Q. Li, X. G. Miao, and L. W. Yin, "ZnS-Sb_2S_3@C Core-double shell polyhedron structure derived from metal-organic framework as anodes for high performance sodium ion batteries," *ACS Nano*, vol. 11, no. 6, pp. 6474–6482, 2017.

[18] T. Saito, S. Tsuneda, A. Hirata et al., "Removal of antimony (III) using polyol-ligand-containing porous hollow-fiber membranes," *Separation Science and Technology*, vol. 39, no. 13, pp. 3011–3022, 2004.

[19] Z. Zhao, X. Wang, C. Zhao, X. Zhu, and S. Du, "Adsorption and desorption of antimony acetate on sodium montmorillonite," *Journal of Colloid Interface Science*, vol. 345, no. 2, pp. 154–159, 2010.

[20] J. Xi, M. He, and C. Lin, "Adsorption of antimony(III) and antimony(V) on bentonite: kinetics, thermodynamics and anion competition," *Microchemical Journal*, vol. 97, no. 1, pp. 85–91, 2011.

[21] J. Ma, X. Y. Guo, Y. P. Ying, D. H. Liu, and C. L. Zhong, "Composite ultrafiltration membrane tailored by with highly improved water purification performance," *Chemical Engineering Journal*, vol. 313, pp. 890–898, 2017.

[22] Z. Q. Xue, K. Liu, Q. L. Liu et al., "Missing-linker metal-organic frameworks for oxygen evolution reaction," *Nature Communications*, vol. 10, no. 1, p. 5048, 2019.

[23] C. H. Wang, X. L. Liu, J. P. Chen, and K. Li, "Superior removal of arsenic from water with zirconium metal-organic framework UiO-66," *Scientific Reports*, vol. 5, no. 1, p. 16613, 2015.

[24] Z. Shao, C. Huang, J. Dang et al., "Modulation of magnetic behavior and Hg^{2+} removal by solvent-assisted linker exchange based on a water-stable 3D MOF," *Chemistry of Materials*, vol. 30, no. 21, pp. 7979–7987, 2018.

[25] S. M. Mao, J. W. Shi, G. T. Sun et al., "Au nanodots@ thiol-UiO66@ ZnIn2S4 nanosheets with significantly enhanced visible-light photocatalytic H2 evolution: The effect of different Au positions on the transfer of electron-hole pairs," *Applied Catalysis B: Environmental*, vol. 282, article 119550, 2021.

[26] Y. H. Tian, Z. C. Yu, L. Y. Cao, X. L. Zhang, C. H. Sun, and D. W. Wang, "Graphene oxide: an emerging electromaterial for energy storage and conversion," *Journal of Energy Chemistry*, vol. 55, pp. 323–344, 2021.

[27] X. C. Zhang, X. Zhang, H. R. Yuan et al., "CoNi nanoparticles encapsulated by nitrogen-doped carbon nanotube arrays on reduced graphene oxide sheets for electromagnetic wave absorption," *Chemical Engineering Journal*, vol. 383, article 123208, 2020.

[28] K. Violetta, B. Andrzej, P. Danuta et al., "Derivatives of graphene oxide as potential drug carriers," *Journal of Nanoscience and Nanotechnology*, vol. 19, no. 5, pp. 2489–2492, 2019.

[29] H. P. Wu, Y. Y. Yan, J. Feng et al., "Cetylpyridinium bromide/montmorillonite-graphene oxide composite with good antibacterial activity," *Biomedical Materials*, vol. 15, no. 5, article 055002, 2020.

[30] G. Ersan, O. G. Apul, F. Perreault, and T. Karanfil, "Adsorption of organic contaminants by graphene nanosheets: a review," *Water Research*, vol. 126, pp. 385–398, 2017.

[31] W. Peng, H. Li, Y. Liu, and S. Song, "A review on heavy metal ions adsorption from water by graphene oxide and its composites," *Journal of Molecular Liquids*, vol. 230, pp. 496–504, 2017.

[32] J. Wang and B. Chen, "Adsorption and coadsorption of organic pollutants and a heavy metal by graphene oxide and reduced graphene materials," *Chemical Engineering Journal*, vol. 281, pp. 379–388, 2015.

[33] S. Wang, H. Sun, H. M. Ang, and M. O. Tade, "Adsorptive remediation of environmental pollutants using novel graphene-based nanomaterials," *The Chemical Engineering Journal*, vol. 226, pp. 336–347, 2013.

[34] W. M. Liu, X. Q. Wang, C. M. Wang, G. G. Chen, W. L. Sun, and C. T. Zheng, "Green and large-scale preparation of reduced graphene oxide for electroreduction of nitrobenzene to p-aminophenol," *Micro & Nano Letters*, vol. 11, no. 11, pp. 661–665, 2016.

[35] X. D. Du, X. H. Yi, P. Wang, W. Zheng, J. Deng, and C. C. Wang, "Robust photocatalytic reduction of Cr(VI) on UiO-66-NH_2(Zr/Hf) metal-organic framework membrane under sunlight irradiation," *Chemical Engineering Journal*, vol. 356, pp. 393–399, 2019.

[36] L. Lu, Y. Lin, Q. Chai, S. He, and C. Yang, "Removal of acenaphthene by biochar and raw biomass with coexisting heavy metal and phenanthrene," *Colloids and Surfaces A: Physicochemical and Engineering Aspects*, vol. 558, pp. 103–109, 2018.

[37] Y. Lin, C. P. Yang, S. H. Wu, X. Li, Y. J. Chen, and W. L. Yang, "Construction of built-in electric field within silver phosphate photocatalyst for enhanced removal of recalcitrant organic pollutants," *Advanced Functional Materials*, vol. 30, no. 38, article 2002918, 2020.

[38] Y. Lin, S. Wu, C. P. Yang, M. Chen, and X. Li, "Preparation of size-controlled silver phosphate catalysts and their enhanced photocatalysis performance via synergetic effect with MWCNTs and PANI," *Applied Catalysis B: Environmental*, vol. 245, pp. 71–86, 2019.

[39] P. Qi, R. Luo, T. Pichler et al., "Development of a magnetic core-shell Fe3O4@ TA@ UiO-66 microsphere for removal of arsenic (III) and antimony (III) from aqueous solution," *Journal of Hazardous Materials*, vol. 378, article 120721, 2019.

[40] M. Lu, Y. Deng, Y. Luo et al., "Graphene aerogel-metal-organic framework-based electrochemical method for simultaneous

detection of multiple heavy-metal ions," *Analytical Chemistry*, vol. 91, no. 1, pp. 888–895, 2019.

[41] S. S. Chen, C. Hu, C. H. Liu et al., "De novo synthesis of platinum-nanoparticle-encapsulated UiO-66-NH_2 for photocatalytic thin film fabrication with enhanced performance of phenol degradation," *Journal of Hazardous Materials*, vol. 397, article 122431, 2020.

[42] Y. Lin, C. P. Yang, Q. Y. Niu, and S. L. Luo, "Interfacial charge transfer between silver phosphate and W_2N_3 induced by nitrogen vacancies enhances removal of β-lactam antibiotics," *Advanced Functional Materials*, vol. 32, no. 5, p. 2108814, 2022.

[43] X. Wu, H. J. He, W. L. Yang, J. P. Yu, and C. P. Yang, "Efficient removal of atrazine from aqueous solutions using magnetic *Saccharomyces cerevisiae* bionanomaterial," *Applied Microbiology and Biotechnology*, vol. 102, no. 17, pp. 7597–7610, 2018.

[44] L. Fu, S. Wang, G. Lin et al., "Post-functionalization of UiO-66-NH_2 by 2,5-dimercapto-1,3,4-thiadiazole for the high efficient removal of Hg(II) in water," *Journal of Hazardous Materials*, vol. 368, pp. 42–51, 2019.

[45] M. R. Awual, "Efficient phosphate removal from water for controlling eutrophication using novel composite adsorbent," *Journal of Cleaner Production*, vol. 228, pp. 1311–1319, 2019.

[46] H. Azarpira, Y. Mahdavi, and D. Balarak, "Removal of Cd(II) by adsorption on agricultural waste biomass," *Der Pharma Chemica*, vol. 8, no. 12, pp. 61–67, 2016.

[47] F. Zhu, Y. M. Zheng, B. G. Zhang, and Y. R. Dai, "A critical review on the electrospun nanofibrous membranes for the adsorption of heavy metals in water treatment," *Journal of Hazardous Materials*, vol. 401, article 123608, 2021.

[48] D. Balarak, H. Azarpira, and F. K. Mostafapour, "Thermodynamics of removal of cadmium by adsorption on barley husk biomass," *Der Pharma Chemica*, vol. 8, no. 10, pp. 243–247, 2016.

[49] C. Guan, S. M. Liu, C. W. Li, Y. Wang, and Y. X. Zhao, "The temperature effect on the methane and CO_2 adsorption capacities of Illinois coal," *Fuel*, vol. 211, pp. 241–250, 2018.

[50] X. He, F. Deng, T. Shen et al., "Exceptional adsorption of arsenic by zirconium metal-organic frameworks: engineering exploration and mechanism insight," *Journal of Colloid and Interface Science*, vol. 539, pp. 223–234, 2019.

[51] F. Moghimi, A. H. Jafari, H. Yoozbashizadeh, and M. Askari, "Adsorption behavior of Sb(III) in single and binary Sb(III)–Fe(II) systems on cationic ion exchange resin: adsorption equilibrium, kinetic and thermodynamic aspects," *Transactions of Nonferrous Metals Society of China*, vol. 30, no. 1, pp. 236–248, 2020.

[52] P. Yu, H. Q. Wang, R. Y. Bao et al., "Self-assembled sponge-like chitosan/reduced graphene oxide/montmorillonite composite hydrogels without cross-linking of chitosan for effective Cr (VI) sorption," *ACS Sustainable Chemistry & Engineering*, vol. 5, no. 2, pp. 1557–1566, 2016.